


Nutrient Transport Driven by Microbial Active Carpets

Arnold J. T. M. Mathijssen,^{1,*} Francisca Guzmán-Lastra,^{2,3} Andreas Kaiser,⁴ and Hartmut Löwen⁵¹Department of Bioengineering, Stanford University, 443 Via Ortega, Stanford, California 94305, USA²Facultad de Ciencias, Universidad Mayor, Av. Manuel Montt 367, Providencia, Santiago 7500994, Chile³Departamento de Física, FCFM Universidad de Chile, Beauchef 850, Santiago 8370448, Chile⁴Department of Biomedical Engineering, Pennsylvania State University, University Park, Pennsylvania 16802, USA⁵Institut für Theoretische Physik II: Weiche Materie, Heinrich-Heine-Universität, D-40225 Düsseldorf, Germany (Received 25 June 2018; published 11 December 2018)

We demonstrate that active carpets of bacteria or self-propelled colloids generate coherent flows towards the substrate, and propose that these currents provide efficient pathways to replenish nutrients that feed back into activity. A full theory is developed in terms of gradients in the active matter density and velocity, and applied to bacterial turbulence, topological defects and clustering. Currents with complex spatio-temporal patterns are obtained, which are tunable through confinement. Our findings show that diversity in carpet architecture is essential to maintain biofunctionality.

DOI: 10.1103/PhysRevLett.121.248101

The collective motion of microorganisms and active colloids has sparked great interest, as biological functions can emerge from self-organization of local power injection [1–9]. To sustain these processes, self-propelled particles increase nutrient uptake [10–13] and redistribute oxygen [14] by hydrodynamically enhanced mixing [15–17], bioconvection [18–20], and particle entrainment [21–24]. The vast majority of these flow-driving swimmers accumulate at surfaces [25–35], at concentrations an order of magnitude larger than in the bulk [25,27,30], and thus form “active carpets.” Instead of wall attachment, these freely roaming carpets are stabilized by mutual cell attraction or chemotaxis. However, this crowding drains reserves rapidly, and renewal is restricted by the boundary [36], so biofunctionality is curtailed. Moreover, swimmer-generated flows cancel each other in the case of homogeneous coverage, by symmetry, so supply of nutrients is limited by diffusion. A steady advection changes this situation radically; it opens effective pathways for resource replenishment and reinforces activity.

In this Letter, we demonstrate that such coherent transport arises from gradients in density, activity, or orientation, which emerge naturally from the long-ranged order in collective behavior [37], such as in bacterial vortex arrays [38–42], bacterial turbulence [43–49], and giant density fluctuations [6,50–54]. Topology and geometry play a crucial role in these living fluids [2,55–59], providing a bridge with material sciences and cell biology [9,60]. We focus on bacteria as a concrete example, but this theory applies to the broader class of active carpets to which no external forces and torques are applied.

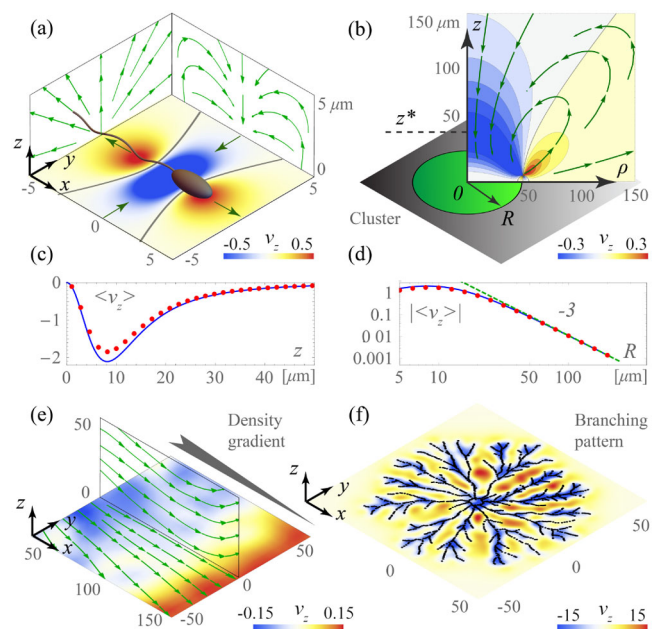


FIG. 1. Currents generated by clusters and density gradients, in $\mu\text{m/s}$. (a) Individual bacterial flow, shown for $z = 5 \mu\text{m}$ (top view), $x = \pm 5 \mu\text{m}$ (front view), $y = \pm 5 \mu\text{m}$ (side view). (b) Bacterial cluster flow, $\langle v(\rho, z) \rangle$, with uniform density $n = 0.1/\mu\text{m}^2$ and size $R = 50 \mu\text{m}$. (c) Vertical flow as a function of z , evaluated at $\rho = 0$ and $R = 10 \mu\text{m}$, obtained numerically (red points) and analytically [blue lines, Eq. (3)]. (d) Same; as a function of R , evaluated at $\rho = 0$ and $z = 10 \mu\text{m}$. (e) Bacterial density gradient, simulated with $N = 12500$ and $R = 200 \mu\text{m}$, shown for the planes $z = 20 \mu\text{m}$ (top view) and $y = 0$. (f) (enlarged in the Supplemental Material [64], Fig. 1) Bacteria arranged in a branching pattern, simulated with $N = 1800$ cells (black points), shown for $z = 5 \mu\text{m}$ (top view).

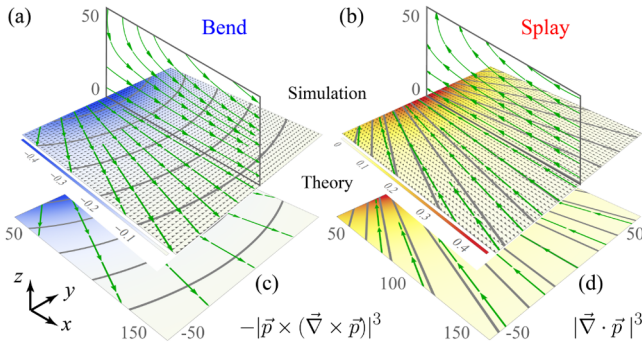


FIG. 2. Flows generated by gradients in the director field. (a) “Bend-type” gradients: bacteria are oriented along circles centered at the origin. (b) “Splay-type” gradients: orientations along the corresponding radial lines. We simulate $N \sim 200000$ swimmers (gray arrows) arranged on a large uniform lattice with $R = 500 \mu\text{m}$ and $n = 0.25/\mu\text{m}^2$, so that density gradients and edge effects are negligible. Colors indicate flows in the z direction, in $\mu\text{m/s}$, evaluated for the plane $z = 20 \mu\text{m}$, and green arrows show stream lines, also for $y = 0$. (c),(d) Corresponding theoretical estimates (6), (7).

First, we show that a bacterial cluster, despite random orientations, creates a net nutrient transport towards the surface. Second, in uniform-density carpets, gradients in swimmer orientation produce flows instead. We derive and implement these to topological defects commonly found in living fluids. Combining these fundamental ingredients, the nutrient transport by vortex arrays and bacterial turbulence are evaluated, and the spatiotemporal correlations of the flows compared to the collective dynamics.

Individual swimmer flows.—We consider a colony of microswimmers with balanced propulsion and drag forces. These are located at \mathbf{r}_s and oriented along \mathbf{p} parallel to a solid surface, which is fixed at $z = 0$ in Cartesian coordinates. Each swimmer generates a flow $\mathbf{u}(\mathbf{r})$ that can displace nutrients, represented by a tracer particle located at \mathbf{r} . At low Reynolds numbers, and for distances $d = |\mathbf{r} - \mathbf{r}_s|$ larger than a few body lengths, this individual flow is well described by a Stokes dipole aligned with the swimming direction [3,61], given by

$$\mathbf{u}(\mathbf{r}, \mathbf{r}_s, \mathbf{p}) = \kappa[(\mathbf{p} \cdot \nabla_s) \mathcal{B}(\mathbf{r}, \mathbf{r}_s)] \cdot \mathbf{p}, \quad (1)$$

where the dipole strength is $|\kappa| \sim 3v_s a_s^2/4$ in terms of the swimmer’s speed v_s and size a_s [23]. The no-slip condition at the wall is accounted for using the Blake tensor $\mathcal{B}(\mathbf{r}, \mathbf{r}_s)$ formalism [62,63] (see Supplemental Material [64], Sec. 1). Throughout this Letter, as an example, we use swimmer height $h = z_s = 1 \mu\text{m}$ and dipole moment $\kappa = 30 \mu\text{m}^3/\text{s}$ for the pusher *E. coli* [61].

Figure 1(a) shows the resulting flow driven by a single bacterium. Nutrients are attracted towards the surface directly above the swimmer (blue regions), but pushed upwards in front of and behind the cell (red regions). The

net flux across any plane in z vanishes due to the incompressibility of the liquid, $\int \mathbf{u} dx dy = 0$, but across a plane recirculating vortices can emerge (green stream lines). For pullers, $\kappa < 0$, the flow direction is inverted. Taken together, the average flow velocity due to all swimmers on the surface combined is

$$\langle \mathbf{v}(\mathbf{r}) \rangle = \int \mathbf{u}(\mathbf{r}, \mathbf{r}_s, \mathbf{p}) f(\mathbf{r}_s, \mathbf{p}) d\mathbf{r}_s d\mathbf{p}, \quad (2)$$

where f is the probability density of finding a swimmer at position \mathbf{r}_s and orientation \mathbf{p} .

Clusters and density gradients.—We examine a cluster of N bacteria that assemble around a chemoattractant (movie S1 [64]). Remarkably, this active carpet generates a steady current that brings nutrients down towards the surface. To analyze this, we first imagine a circular cluster of radius R centered at the origin with constant density, $n = N/(\pi R^2)$, and uniformly distributed swimmer orientations in the plane. The total flow, derived in the Supplemental Material [64] Sec. 2A and shown in Fig. 1(b), is found by inserting this profile, $f \propto (n/2\pi)$, into Eq. (2). As in the movie, this yields a down-welling region for all lateral distances $\rho < R$ and all heights $z > h$, where $\rho = \sqrt{x^2 + y^2}$, despite the random swimmer orientations and thermal particle diffusion. Subsequently, the nutrients move from the center to the edge of the cluster, to $\rho > R$, where incompressibility demands that liquid be transported back up, causing a large toroidal recirculation. Directly above the cluster, along the z axis and in the limit $z \gg h$, the result simplifies to the mean drift velocity

$$\langle \mathbf{v}(z, R) \rangle = -12\pi n h \kappa \frac{z^2 R^2}{(z^2 + R^2)^{5/2}} \hat{\mathbf{z}}. \quad (3)$$

For a typical bacterial density, $n \sim 0.1/\mu\text{m}^2$ [31] and cluster size $R \sim 50 \mu\text{m}$ we expect significant nutrient transport up to $\langle \mathbf{v}(z^*) \rangle \sim 25 \mu\text{m}/\text{min}$ [Figs. 1(b) and 1(c)]. This can be orders of magnitude larger than sedimentation velocities for micron-sized particles. Compared to diffusion the Péclet number is large, $\text{Pe} = (vR/D) \sim 48$, and the transport is additive over time. Moreover, flows are $\sim 2\times$ stronger for more realistic Gaussian clusters (Supplemental Material [64], Sec. 2B).

Counterintuitively, larger homogeneous clusters do not transport faster. To be precise, in the thermodynamic limit where $R, N \rightarrow \infty$ with constant n , the individual swimmer flows cancel each other out, on average, so the surface attraction vanishes. Indeed, the mean flow [Eq. (3)] decays as $1/R^3$ in this limit [Fig. 1(d)]. Maximizing $\langle \mathbf{v}(z, R) \rangle$ with respect to R , for a given distance from the surface z , we obtain the optimal cluster size $R^* = \sqrt{2/3}z$.

More generally, all gradients in swimmer density or activity can drive currents. To see this we simulate a cluster with a linearly decreasing density (Supplemental Material

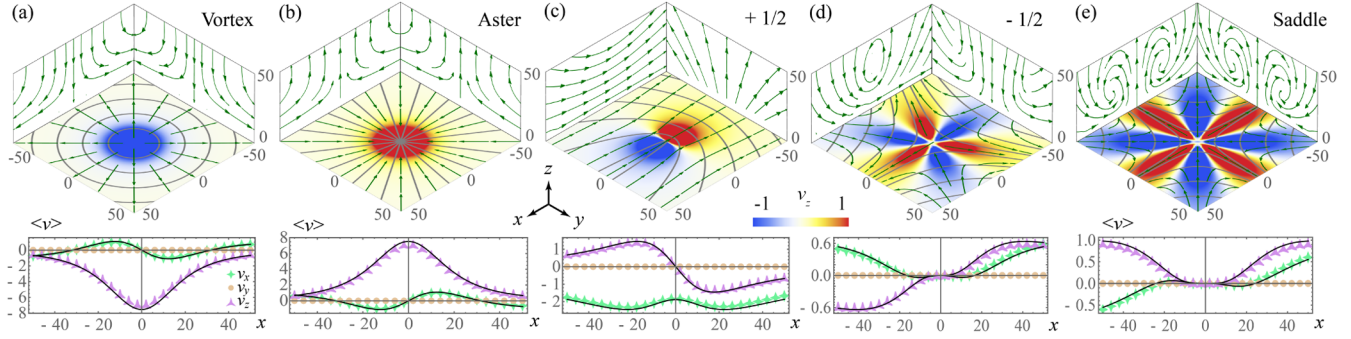


FIG. 3. Defects in the director field generate strong flows because of large orientation gradients. Swimmers are arranged in a dense uniform lattice with orientation $\phi_s = \phi_0 + m\theta$ (gray lines). Upper panels: Colors indicate vertical flows in $\mu\text{m/s}$, simulated for the plane $z = 5 \mu\text{m}$, and green arrows are stream lines, also for the planes $x, y = -50 \mu\text{m}$. (a) Vortex defect with $(m, \phi_0) = (1, \pi/2)$. (b) Aster defect with $(1, 0)$. (c) Plus half defect with $(\frac{1}{2}, 0)$. (d) Minus half defect with $(-\frac{1}{2}, 0)$. (e) Saddle defect with $(-1, 0)$. Lower panels: Flows in $\mu\text{m/s}$ for the plane $y = 0$, obtained numerically (markers) and analytically (lines).

[64], Sec. 5C). As before, this generates a horizontal flow along the gradient with down-welling at the high end [Fig. 1(e)].

Using this information, one can also predict transport driven by clusters of a more complex morphology. Figure 1(f) depicts flows generated by bacteria arranged in a branching pattern (Supplemental Material [64] Sec. 5D). In agreement with the previous simplified cases, flows move downwards to the high-density regions, the branches. This configuration is of course arbitrary, but serves to emphasize the robustness with respect to cluster shape.

An important prerequisite for steady flows is that gradients are sustained. Stable gradients in metabolism can arise by, e.g., local nutrient hot spots, and density gradients by chemotaxis or light control [93–96]. To quantify this, we analyze the stability of a cluster around chemoattractant (Supplemental Material [64] Sec. 6). While we considered an instantaneous swimmer distribution above, we explicitly model their dynamics here, together with rotational (or run-tumble) fluctuations D_r . We find that with increasing chemotactic strength, Ω_c , a stable cluster forms and a net nutrient flux emerges, which saturates when $\Omega_c > D_r$.

Orientation gradients.—In the previous scenario with random orientations, the mean flows vanish in the absence of gradients in density. Furthermore, if all swimmers are oriented in the same direction, through collective motion or alignment interactions, then the currents also cancel in the thermodynamic limit (Supplemental Material [64] Sec. 3A). However, gradients in swimmer orientation give rise to a second source of flow generation.

To classify the relevant orientation derivatives, it is important to note that the swimmer flow [Eq. (1)] is nematicially symmetric [Fig. 1(a)], i.e., invariant under $\mathbf{p} \rightarrow -\mathbf{p}$. Hence, the only first-order derivatives that obey this symmetry in a 2D active carpet are, expressed in liquid crystal terminology [97], the “bend” and “splay” contributions,

$$B = [\mathbf{p} \times (\nabla_s \times \mathbf{p})]^2, \quad (4)$$

$$S = (\nabla_s \cdot \mathbf{p})^2. \quad (5)$$

The effect of these gradients is illustrated in Fig. 2. We consider actives particles that swim collectively (a) in concentric circles, $\phi_s = \theta + (\pi/2)$, or (b) towards a chemoattractant source, $\phi_s = \theta$, where $\phi_s = \arctan(p_y/p_x)$ and $\theta = \arctan(y/x)$, and they are spread out uniformly in space to minimise swimmer density gradients (Supplemental Material [64] Sec. 5E). In both cases the orientation gradients decay with distance from the center quadratically; for (a) we have $B(\rho) = 1/\rho^2$ and $S(\rho) = 0$, and vice versa for (b). Then, a strong correlation is observed between bend gradients and liquid moving downwards and outwards. Conversely, splay gradients drive flows inwards and upwards.

To make analytical progress, we realize that it is not always possible to find a general formula for the *local* flow in terms of the gradients, $\langle \mathbf{v} \rangle(\mathbf{r}) = \chi(B, S)$, because the velocity is generated by a *region* of swimmers in which the gradients vary. These variations increase for larger z values as the number of equidistant swimmers, i.e., this region of influence, grows. However, the gradients are approximately constant far from the circle center, when $z \ll \rho$, so we can couple the gradients and flows in that area [Figs. 2(a), 2(b)]. Therefore, by expanding the mean current [Eq. (2)] in terms of $1/\rho$ (Supplemental Material [64], Secs. 3B, 3C), we find the first-order contributions to the horizontal and vertical flows due to bend and splay gradients,

$$\langle v_\rho \rangle \approx 8\pi n h \kappa (\sqrt{B(\rho)} - \sqrt{S(\rho)}), \quad (6)$$

$$\langle v_z \rangle \approx -8\pi n h \kappa z^2 ([B(\rho)]^{3/2} - [S(\rho)]^{3/2}). \quad (7)$$

This approximation, shown in Fig. 2(c,d), offers a good agreement with its numerical counterpart. It also follows

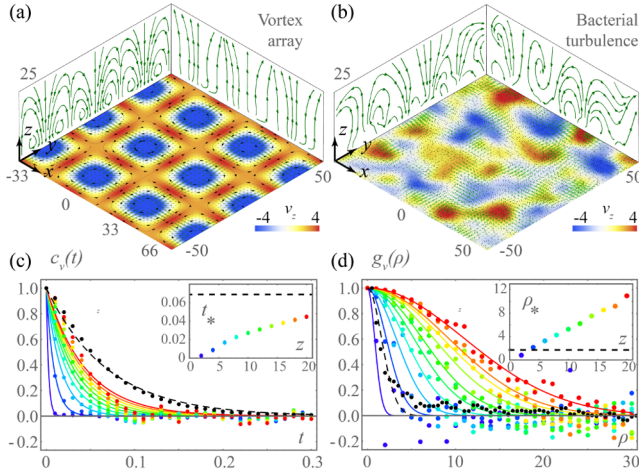


FIG. 4. Flows created by collectively moving swimmers. (a) (enlarged in the Supplemental Material [64], Fig. 2) Taylor-Green vortex pattern with unit cell size $\lambda = 33 \mu\text{m}$, and uniform swimmer density $n = 0.25/\mu\text{m}^2$. (b) (enlarged in the Supplemental Material [64], Fig. 4) Bacterial turbulence, simulated with the SPR model with aspect ratio $a = 5$, packing fraction $\Phi = 0.7$ and $n = 0.25/\mu\text{m}^2$. (a),(b) Colors indicate vertical flows in $\mu\text{m/s}$, simulated for $z = 10 \mu\text{m}$. Green arrows are stream lines and black arrows the swimmer orientations. (c),(d) Bacterial turbulence. Temporal and spatial correlation functions of v_z , respectively, for $z \in [2, 20]$ (blue-red), with corresponding correlations of swimmer orientation (dashed black). Fits (solid lines) provide the correlation time (t_*) and length (ρ_*). Insets show these swimmer (dashed) and flow (blue-red, fits in gray) correlations against height.

that for weak gradients, the horizontal flows are stronger than the vertical transport.

Topological defects.—Like we saw for density gradients, it is now possible to interpret more complex carpet designs in terms of the fundamental ingredients, bend and splay. The first nontrivial orientation patterns with significant orientation gradients are the lowest-order topological defects (Fig. 3). Their director fields are defined as $\phi_s = \phi_0 + m\theta$, where ϕ_0 is a phase angle and $m = \pm\frac{1}{2}, \pm 1, \pm\frac{3}{2}, \dots$ is the topological charge [97]. Because these defect arrangements are well characterized mathematically, it is possible to find analytical solutions for the flows they generate (Supplemental Material [64], Sec. IV).

Swimmers with polar order feature integer charge defects. For $m = 1$ [Figs. 3(a) and 3(b)], there is a continuous transition from nutrient attraction near “vortex” defects ($\phi_0 = (\pi/2)$), via no flow “spiral” defects ($\phi_0 = (\pi/4)$), to repulsion near “aster” defects ($\phi_0 = 0$),

$$\langle v_z \rangle^{m=1} = 8\pi n h \kappa \frac{z^2 \cos(2\phi_0)}{(\rho^2 + z^2)^{3/2}}. \quad (8)$$

Active particles with nematic order feature half-integer charges. Near an $m = \frac{1}{2}$ defect [Fig. 3(c)], cooperation between bend and splay gradients drives horizontal

currents, outwards from the bend curvature. The flows in z follow from recirculation, down towards the defect and back up again, with extrema at $\rho = z/\sqrt{2}$. Also near $m = -\frac{1}{2}$ defects and near “saddle” defects, $m = -1$, the horizontal flows move in towards the convex side of the bends and out in the regions of converging splay [Figs. 3(d) and 3(e)]. In all cases, the calculated flows (Supplemental Material [64], Sec. IV) agree well with the simulated ones (Fig. 3, lower panels).

An important observation is that splay gradients [divergence of \mathbf{p} in Eq. (5)] and density gradients are coupled in time, via motility. Specifically, bacteria can accumulate or deplete from defects, as observed in liquid crystals [98]. Therefore, vortex defects [Fig. 3(a)] remain stable over time, but steady states of aster defects [Fig. 3(b)] must feature more complex dynamics, such as defect ordering [99] or ejection of swimmers from the carpet into the bulk. Otherwise the defects can be motile, with time-dependent flows, as we discuss below for bacterial turbulence.

Vortex arrays.—The topological building blocks can be used to comprehend the currents created by active carpets featuring collective motion. Particularly common in nature, and microfluidically controllable, are vortex patterns that bacteria or spermatozoa at high surface densities can self-organize into [38–42]. Note, high surface densities go hand in hand with association and dissociation of swimmers in the bulk [5]. Therefore, even if bulk swimmers are an order of magnitude more sparse [25,27], they will also generate diffusive flows [15–17].

We first consider a Taylor-Green vortex (TGV) carpet, which periodically features vortex and saddle defects ($m = \pm 1$) at the center and corners of the unit cell, respectively [Fig. 4(a), Supplemental Material [64] Sec. 5F]. Nutrients are attracted down to the vortex centers [locally described by Eq. (8)], and recirculated upwards with fourfold symmetry at the face centers of the unit cell, in agreement with the individual defect flows [Figs. 3(a), 3(e)]. Changing the vortex size with confinement can therefore tune the flows.

Bacterial turbulence.—Similarly, we consider the more complex patterns generated by bacterial turbulence [43–49]. Their collective dynamics are simulated using the Self-Propelled Rod (SPR) model [49] to determine swimmer positions and orientation (movie S2, Supplemental Material [64], Secs. 7A, 7B). Because of the high volume fraction, density gradients remain negligible but orientation gradients are abundant. Hence, recirculatory currents are generated, as shown in Fig. 4(b). Weak flows occur in the regions where swimmers are aligned with each other (Supplemental Material [64], Sec. 3A), but defects give rise to strong bend and splay gradients and thus nutrient transport.

Movies S3–S5 show how these currents develop during the onset of turbulence, giving top views at $z = 10, 25 \mu\text{m}$, respectively, and a side view for the cross section $y = 0$. Interestingly, further from the active carpet

the down-welling and up-welling regions are slower but larger. We quantify this by computing the temporal and spatial correlation functions, $c_{v_z}(t)$ and $g_{v_z}(\rho)$, for different heights z (Supplemental Material [64], Secs. 7C, 7D). Hence, we obtain the correlation time $t_*(z)$ and correlation length $\rho_*(z)$ from their fits [Figs. 4(c) and 4(d)]. At short timescales the nutrient transport is ballistic but, of course, after this memory time it is diffusive. Far from the carpet this memory is set by the decorrelation of swimmer orientations (dashed black), but nearby t_* reduces to the mean free time between collisions with individual swimmers. Conversely, the correlation length ρ_* grows linearly with z , and it is not bound by the correlation length of swimmer orientations because the region of influence by more equidistant bacteria grows beyond the turbulent swirl radius. Indeed, the renormalized correlations $g_{v_z}(\rho/z)$ collapse onto one another (Supplemental Material [64], Fig. 5), highlighting the scaling relation of the flow's long rangedness.

Topological analysis of active carpets can be a powerful technique: Knowing only the defect configuration in homogeneous carpets, one can interpolate the director field and thus predict the resulting flows. We describe this for a monolayer of bacteria, but at higher cell densities the carpet could be thicker with multiple layers moving collectively. Our analysis might still apply then, provided the carpet thickness is smaller than the correlation length, before transitioning to 3D turbulence [100,101].

Conclusions.—We studied the emergence of large-scale recirculation by a carpet of force-free actuators. Surprisingly, finite clusters of randomly oriented bacteria drive nondiffusive currents, in contracts with ciliary arrays [102–105] and grafted cells [106–109], where alignment is essential for microbiological transport (Supplemental Material [64] Sec. 2C). Moreover, in the context of diversity in carpet architecture, it might be beneficial for an individual organism not to generate a flow to maximize the collective flux. To consolidate this, a mathematical foundation is derived in terms of gradients in the carpet activity, density, and orientation fields. In nature, stable density gradients or clustering can arise by self-assembly [6,7,53] and chemo-, thermo-, photo-, or rheotaxis [35,110]. Orientation gradients can form through individual actuation or collective instabilities [37,111]. To stabilize these, topological constraints are key, through defect ordering [99] or confinement by liquid drops [112] and spherical manifolds [113]. Experimental realizations may be achieved by chemoattractants, thermokinetic, or light-controlled coordination [93–96]. Lithographic surface patterning and rectification [114–117] could also make complex flux patterns when correcting for disturbance flows due to cell-wall interactions [3–5]. Hence, these currents may be employed to drive active flow networks [118] and provide understanding for transport by complex-shaped clusters, for bacterial turbulence [43–49], and biofilm architecture [119].

We would like to thank Manu Prakash and Deepak Krishnamurthy for helpful discussions. A. M. acknowledges funding from the Human Frontier Science Program (Fellowship LT001670/2017). F. G. L. acknowledges Millennium Nucleus “Physics of active matter” of the Millennium Scientific Initiative of the Ministry of Economy, Development and Tourism, Chile. H. L. acknowledges support from the Deutsche Forschungsgemeinschaft, DFG Project No. LO 418/17-2.

*To whom all correspondence should be addressed.
amath@stanford.edu

- [1] T. Vicsek and A. Zafeiris, Collective motion, *Phys. Rep.* **517**, 71 (2012).
- [2] M. Marchetti, J. Joanny, S. Ramaswamy, T. Liverpool, J. Prost, M. Rao, and R. Simha, Hydrodynamics of soft active matter, *Rev. Mod. Phys.* **85**, 1143 (2013).
- [3] E. Lauga and T. R. Powers, The hydrodynamics of swimming microorganisms, *Rep. Prog. Phys.* **72**, 096601 (2009).
- [4] D. L. Koch and G. Subramanian, Collective hydrodynamics of swimming microorganisms: living fluids, *Annu. Rev. Fluid Mech.* **43**, 637 (2011).
- [5] J. Elgeti, R. G. Winkler, and G. Gompper, Physics of microswimmers—single particle motion and collective behavior: A review, *Rep. Prog. Phys.* **78**, 056601 (2015).
- [6] M. Cates and J. Tailleur, Motility-induced phase separation, *Annu. Rev. Condens. Matter Phys.* **6**, 219 (2015).
- [7] C. Bechinger, R. Di Leonardo, H. Löwen, C. Reichhardt, G. Volpe, and G. Volpe, Active particles in complex and crowded environments, *Rev. Mod. Phys.* **88**, 045006 (2016).
- [8] A. Zöttl and H. Stark, Emergent behavior in active colloids, *J. Phys. Condens. Matter* **28**, 253001 (2016).
- [9] D. Needleman and Z. Dogic, Active matter at the interface between materials science and cell biology, *Nat. Rev. Mater.* **2**, 17048 (2017).
- [10] V. Magar, T. Goto, and T. J. Pedley, Nutrient uptake by a self-propelled steady squirmer, *Q. J. Mech. Appl. Math.* **56**, 65 (2003).
- [11] M. B. Short, C. A. Solari, S. Ganguly, T. R. Powers, J. O. Kessler, and R. E. Goldstein, Flows driven by flagella of multicellular organisms enhance long-range molecular transport, *Proc. Natl. Acad. Sci. U.S.A.* **103**, 8315 (2006).
- [12] S. Michelin and E. Lauga, Optimal feeding is optimal swimming for all Péclet numbers, *Phys. Fluids* **23**, 101901 (2011).
- [13] D. Tam and A. E. Hosoi, Optimal feeding and swimming gaits of biflagellated organisms, *Proc. Natl. Acad. Sci. U.S.A.* **108**, 1001 (2011).
- [14] I. Tuval, L. Cisneros, C. Dombrowski, C. W. Wolgemuth, J. O. Kessler, and R. E. Goldstein, Bacterial swimming and oxygen transport near contact lines, *Proc. Natl. Acad. Sci. U.S.A.* **102**, 2277 (2005).
- [15] X.-L. Wu and A. Libchaber, Particle diffusion in a quasi-two-dimensional bacterial bath, *Phys. Rev. Lett.* **84**, 3017 (2000).

- [16] M. J. Kim and K. S. Breuer, Enhanced diffusion due to motile bacteria, *Phys. Fluids* **16**, L78 (2004).
- [17] J.-L. Thiffeault and S. Childress, Stirring by swimming bodies, *Phys. Lett. A* **374**, 3487 (2010).
- [18] T. Pedley, N. Hill, and J. Kessler, The growth of bioconvection patterns in a uniform suspension of gyrotactic micro-organisms, *J. Fluid Mech.* **195**, 223 (1988).
- [19] N. Hill and T. J. Pedley, Bioconvection, *Fluid Dyn. Res.* **37**, 1 (2005).
- [20] A. Karimi and A. Ardekani, Gyrotactic bioconvection at pycnoclines, *J. Fluid Mech.* **733**, 245 (2013).
- [21] D. O. Pushkin, H. Shum, and J. M. Yeomans, Fluid transport by individual microswimmers, *J. Fluid Mech.* **726**, 5 (2013).
- [22] R. Jeanneret, D. O. Pushkin, V. Kantsler, and M. Polin, Entrainment dominates the interaction of microalgae with micron-sized objects, *Nat. Commun.* **7**, 12518 (2016).
- [23] A. J. T. M. Mathijssen, R. Jeanneret, and M. Polin, Universal entrainment mechanism controls contact times with motile cells, *Phys. Rev. Fluids* **3**, 033103 (2018).
- [24] L. Vaccari, M. Molaei, R. L. Leheny, and K. J. Stebe, Cargo carrying bacteria at interfaces, *Soft Matter* **14**, 5643 (2018).
- [25] A. P. Berke, L. Turner, H. C. Berg, and E. Lauga, Hydrodynamic Attraction of Swimming Microorganisms by Surfaces, *Phys. Rev. Lett.* **101**, 038102 (2008).
- [26] G. Li and J. X. Tang, Accumulation of Microswimmers Near a Surface Mediated by Collision and Rotational Brownian Motion, *Phys. Rev. Lett.* **103**, 078101 (2009).
- [27] M. Molaei, M. Barry, R. Stocker, and J. Sheng, Failed escape: Solid Surfaces Prevent Tumbling of *Escherichia Coli*, *Phys. Rev. Lett.* **113**, 068103 (2014).
- [28] O. Sipoș, K. Nagy, R. Di Leonardo, and P. Galajda, Hydrodynamic Trapping of Swimming Bacteria by Convex Walls, *Phys. Rev. Lett.* **114**, 258104 (2015).
- [29] J. Elgeti and G. Gompper, Run-and-tumble dynamics of self-propelled particles in confinement, *Eur. Phys. Lett.* **109**, 58003 (2015).
- [30] A. J. T. M. Mathijssen, A. Doostmohammadi, J. M. Yeomans, and T. N. Shendruk, Hotspots of boundary accumulation: dynamics and statistics of micro-swimmers in flowing films, *J. R. Soc. Interface* **13**, 20150936 (2016).
- [31] N. Figueroa-Morales, G. Miño, A. Rivera, R. Caballero, E. Clément, E. Altshuler, and A. Lindner, Living on the edge: Transfer and traffic of *E. coli* in a confined flow, *Soft Matter* **11**, 6284 (2015).
- [32] C. Jin, B. V. Hokmabad, K. A. Baldwin, and C. C. Maass, Chemotactic droplet swimmers in complex geometries, *J. Phys. Condens. Matter* **30**, 054003 (2018).
- [33] A. Daddi-Moussa-Ider, M. Lisicki, A. J. T. M. Mathijssen, C. Hoell, S. Goh, J. Błazdziewicz, A. M. Menzel, and H. Löwen, State diagram of a three-sphere microswimmer in a channel, *J. Phys. Condens. Matter* **30**, 254004 (2018).
- [34] T. Ohmura, Y. Nishigami, A. Taniguchi, S. Nonaka, J. Manabe, T. Ishikawa, and M. Ichikawa, Simple mechanosense and response of cilia motion reveal the intrinsic habits of ciliates, *Proc. Natl. Acad. Sci. U.S.A.* **115**, 3231 (2018).
- [35] A. J. T. M. Mathijssen, N. Figueroa-Morales, G. Junot, E. Clément, A. Lindner, and A. Zöttl, Oscillatory surface rheotaxis of swimming *E. coli* bacteria, [arXiv:1803.01743](https://arxiv.org/abs/1803.01743).
- [36] A. J. T. M. Mathijssen, D. O. Pushkin, and J. M. Yeomans, Tracer trajectories and displacement due to a microswimmer near a surface, *J. Fluid Mech.* **773**, 498 (2015).
- [37] J. Toner and Y. Tu, Long-Range Order in a Two-Dimensional Dynamical XY Model: How Birds Fly Together, *Phys. Rev. Lett.* **75**, 4326 (1995).
- [38] I. H. Riedel, K. Kruse, and J. Howard, A self-organized vortex array of hydrodynamically entrained sperm cells, *Science* **309**, 300 (2005).
- [39] E. Lushi, H. Wioland, and R. E. Goldstein, Fluid flows created by swimming bacteria drive self-organization in confined suspensions, *Proc. Natl. Acad. Sci. U.S.A.* **111**, 9733 (2014).
- [40] C. J. Ingham and E. B. Jacob, Swarming and complex pattern formation in *paenibacillus* vortex studied by imaging and tracking cells, *BMC Microbiol.* **8**, 36 (2008).
- [41] H. Wioland, F. G. Woodhouse, J. Dunkel, J. O. Kessler, and R. E. Goldstein, Confinement Stabilizes a Bacterial Suspension into a Spiral Vortex, *Phys. Rev. Lett.* **110**, 268102 (2013).
- [42] H. Wioland, F. G. Woodhouse, J. Dunkel, and R. E. Goldstein, Ferromagnetic and antiferromagnetic order in bacterial vortex lattices, *Nat. Phys.* **12**, 341 (2016).
- [43] C. Dombrowski, L. Cisneros, S. Chatkaew, R. E. Goldstein, and J. O. Kessler, Self-Concentration and Large-Scale Coherence in Bacterial Dynamics, *Phys. Rev. Lett.* **93**, 098103 (2004).
- [44] A. Sokolov, I. S. Aranson, J. O. Kessler, and R. E. Goldstein, Concentration Dependence of the Collective Dynamics of Swimming Bacteria, *Phys. Rev. Lett.* **98**, 158102 (2007).
- [45] H.-P. Zhang, A. Beer, E.-L. Florin, and H. L. Swinney, Collective motion and density fluctuations in bacterial colonies, *Proc. Natl. Acad. Sci. U.S.A.* **107**, 13626 (2010).
- [46] L. H. Cisneros, R. Cortez, C. Dombrowski, R. E. Goldstein, and J. O. Kessler, Fluid dynamics of self-propelled microorganisms, from individuals to concentrated populations, *Anim. Locomot.* **43**, 99 (2010).
- [47] A. Sokolov and I. S. Aranson, Physical Properties of Collective Motion in Suspensions of Bacteria, *Phys. Rev. Lett.* **109**, 248109 (2012).
- [48] J. Dunkel, S. Heidenreich, K. Drescher, H. H. Wensink, M. Bär, and R. E. Goldstein, Fluid Dynamics of Bacterial Turbulence, *Phys. Rev. Lett.* **110**, 228102 (2013).
- [49] H. H. Wensink, J. Dunkel, S. Heidenreich, K. Drescher, R. E. Goldstein, H. Löwen, and J. M. Yeomans, Mesoscale turbulence in living fluids, *Proc. Natl. Acad. Sci. U.S.A.* **109**, 14308 (2012).
- [50] V. Narayan, S. Ramaswamy, and N. Menon, Long-lived giant number fluctuations in a swarming granular nematic, *Science* **317**, 105 (2007).
- [51] Y. Fily and M. C. Marchetti, Athermal Phase Separation of Self-Propelled Particles with no Alignment, *Phys. Rev. Lett.* **108**, 235702 (2012).
- [52] I. Buttinoni, J. Bialké, F. Kümmel, H. Löwen, C. Bechinger, and T. Speck, Dynamical Clustering and Phase Separation in Suspensions of Self-Propelled Colloidal Particles, *Phys. Rev. Lett.* **110**, 238301 (2013).

- [53] N. Sepúlveda and R. Soto, Wetting Transitions Displayed by Persistent Active Particles, *Phys. Rev. Lett.* **119**, 078001 (2017).
- [54] C. Reichhardt and C. Reichhardt, Clogging and depinning of ballistic active matter systems in disordered media, *Phys. Rev. E* **97**, 052613 (2018).
- [55] G. Tóth, C. Denniston, and J. M. Yeomans, Hydrodynamics of Topological Defects in Nematic Liquid Crystals, *Phys. Rev. Lett.* **88**, 105504 (2002).
- [56] J. Elgeti, M. Cates, and D. Marenduzzo, Defect Hydrodynamics in 2D Polar Active Fluids, *Soft Matter* **7**, 3177 (2011).
- [57] T. Sanchez, D. T. Chen, S. J. DeCamp, M. Heymann, and Z. Dogic, Spontaneous motion in hierarchically assembled active matter, *Nature (London)* **491**, 431 (2012).
- [58] F. C. Keber, E. Loiseau, T. Sanchez, S. J. DeCamp, L. Giomi, M. J. Bowick, M. C. Marchetti, Z. Dogic, and A. R. Bausch, Topology and dynamics of active nematic vesicles, *Science* **345**, 1135 (2014).
- [59] L. Giomi, Geometry and Topology of Turbulence in Active Nematics, *Phys. Rev. X* **5**, 031003 (2015).
- [60] T. B. Saw, A. Doostmohammadi, V. Nier, L. Kocgozlu, S. Thampi, Y. Toyama, P. Marcq, C. T. Lim, J. M. Yeomans, and B. Ladoux, Topological defects in epithelia govern cell death and extrusion, *Nature (London)* **544**, 212 (2017).
- [61] K. Drescher, J. Dunkel, L. H. Cisneros, S. Ganguly, and R. E. Goldstein, Fluid dynamics and noise in bacterial cell–cell and cell–surface scattering, *Proc. Natl. Acad. Sci. U.S.A.* **108**, 10940 (2011).
- [62] J. R. Blake, A note on the image system for a Stokeslet in a no-slip boundary, *Math. Proc. Cambridge Philos. Soc.* **70**, 303 (1971).
- [63] A. J. T. M. Mathijssen, A. Doostmohammadi, J. M. Yeomans, and T. N. Shendruk, Hydrodynamics of microswimmers in films, *J. Fluid Mech.* **806**, 35 (2016).
- [64] See Supplemental Material at <http://link.aps.org/supplemental/10.1103/PhysRevLett.121.248101> for details and five supplemental movies, which includes Refs. [6,12,13,15–17,21–23,31,49,62,63,65–92,102–109].
- [65] M. J. Kim and K. S. Breuer, Controlled mixing in microfluidic systems using bacterial chemotaxis, *Anal. Chem.* **79**, 955 (2007).
- [66] Z. Lin, J.-L. Thiffeault, and S. Childress, Stirring by squirmers, *J. Fluid Mech.* **669**, 167 (2011).
- [67] D. O. Pushkin and J. M. Yeomans, Fluid Mixing by Curved Trajectories of Microswimmers, *Phys. Rev. Lett.* **111**, 188101 (2013).
- [68] P. Mueller and J.-L. Thiffeault, Fluid transport and mixing by an unsteady microswimmer, *Phys. Rev. Fluids* **2**, 013103 (2017).
- [69] S. Chandrasekhar, Stochastic problems in physics and astronomy, *Rev. Mod. Phys.* **15**, 1 (1943).
- [70] N. King, M. J. Westbrock, S. L. Young, A. Kuo, M. Abedin, J. Chapman, S. Fairclough, U. Hellsten, Y. Isogai, I. Letunic *et al.*, The genome of the choanoflagellate *Monosiga brevicollis* and the origin of metazoans, *Nature (London)* **451**, 783 (2008).
- [71] M. Roper, M. J. Dayel, R. E. Pepper, and M. A. R. Koehl, Cooperatively Generated Stresslet Flows Supply Fresh Fluid to Multicellular Choanoflagellate Colonies, *Phys. Rev. Lett.* **110**, 228104 (2013).
- [72] L. T. Nielsen, S. S. Asadzadeh, J. Dölger, J. H. Walther, T. Kjørboe, and A. Andersen, Hydrodynamics of microbial filter feeding, *Proc. Natl. Acad. Sci. U.S.A.* **114**, 9373 (2017).
- [73] J. B. Kirkegaard and R. E. Goldstein, Filter-feeding, near-field flows, and the morphologies of colonial choanoflagellates, *Phys. Rev. E* **94**, 052401 (2016).
- [74] J. B. Kirkegaard, A. O. Marron, and R. E. Goldstein, Motility of Colonial Choanoflagellates and the Statistics of Aggregate Random Walkers, *Phys. Rev. Lett.* **116**, 038102 (2016).
- [75] J. Dölger, L. Tor Nielsen, T. Kjørboe, and A. Andersen, Swimming and feeding of mixotrophic biflagellates, *Sci. Rep.* **7**, 39892 (2017).
- [76] W. Gilpin, V. N. Prakash, and M. Prakash, Vortex arrays and ciliary tangles underlie the feeding—swimming trade-off in starfish larvae, *Nat. Phys.* **13**, 380 (2017).
- [77] R. Stocker, J. R. Seymour, A. Samadani, D. E. Hunt, and M. F. Polz, Rapid chemotactic response enables marine bacteria to exploit ephemeral microscale nutrient patches, *Proc. Natl. Acad. Sci. U.S.A.* **105**, 4209 (2008).
- [78] M. Eisenbach, *Chemotaxis* (World Scientific, Singapore, 2004).
- [79] G. H. Wadhams and J. P. Armitage, Making sense of it all: bacterial chemotaxis, *Nat. Rev. Mol. Cell Biol.* **5**, 1024 (2004).
- [80] L. Hall-Stoodley, J. W. Costerton, and P. Stoodley, Bacterial biofilms: from the Natural environment to infectious diseases, *Nat. Rev. Microbiol.* **2**, 95 (2004).
- [81] R. Stocker and J. R. Seymour, Ecology and physics of bacterial chemotaxis in the ocean, *Microbiol. Mol. Biol. Rev.* **76**, 792 (2012).
- [82] P. Romanczuk, M. Bär, W. Ebeling, B. Lindner, and L. Schimansky-Geier, Active Brownian particles, *Eur. Phys. J. Spec. Top.* **202**, 1 (2012).
- [83] E. Ben-Jacob, I. Cohen, and H. Levine, Cooperative self-organization of microorganisms, *Adv. Phys.* **49**, 395 (2000).
- [84] H. C. Berg and D. A. Brown, Chemotaxis in *Escherichia coli* analysed by Three-dimensional Tracking, *Nature (London)* **239**, 500 (1972).
- [85] N. Mittal, E. O. Budrene, M. P. Brenner, and A. Van Oudenaarden, Motility of *Escherichia coli* cells in clusters formed by chemotactic aggregation, *Proc. Natl. Acad. Sci. U.S.A.* **100**, 13259 (2003).
- [86] J. Saragosti, P. Silberzan, and A. Buguin, Modeling *E. coli* tumbles by rotational diffusion. Implications for chemotaxis, *PLoS One* **7**, e35412 (2012).
- [87] M. E. Cates and J. Tailleur, When are active Brownian particles and run-and-tumble particles equivalent? Consequences for motility-induced phase separation, *Eur. Phys. Lett.* **101**, 20010 (2013).
- [88] P. Romanczuk, U. Erdmann, H. Engel, and L. Schimansky-Geier, Beyond the Keller-Segel model, *Eur. Phys. J. Spec. Top.* **157**, 61 (2008).
- [89] F. J. Sevilla and M. Sandoval, Smoluchowski diffusion equation for active Brownian swimmers, *Phys. Rev. E* **91**, 052150 (2015).

- [90] H. H. Wensink and H. Löwen, Emergent states in dense systems of active rods: from swarming to turbulence, *J. Phys. Condens. Matter* **24**, 464130 (2012).
- [91] T. Kirchhoff, H. Löwen, and R. Klein, Dynamical correlations in suspensions of charged rodlike macromolecules, *Phys. Rev. E* **53**, 5011 (1996).
- [92] M. M. Tirado, C. L. Martínez, and J. G. de la Torre, Comparison of theories for the translational and rotational diffusion coefficients of rod-like macromolecules. Application to short DNA fragments, *J. Chem. Phys.* **81**, 2047 (1984).
- [93] E. Steager, C.-B. Kim, J. Patel, S. Bith, C. Naik, L. Reber, and M. J. Kim, Control of microfabricated structures powered by flagellated bacteria using phototaxis, *Appl. Phys. Lett.* **90**, 263901 (2007).
- [94] J. Palacci, S. Sacanna, A. P. Steinberg, D. J. Pine, and P. M. Chaikin, Living crystals of light-activated colloidal surfers, *Science* **339**, 936 (2013).
- [95] J. Arlt, V. A. Martinez, A. Dawson, T. Pilizota, and W. C. Poon, Painting with light-powered bacteria, *Nat. Commun.* **9**, 768 (2018).
- [96] G. Frangipane, D. Dell'Arciprete, S. Petracchini, C. Maggi, F. Saglimbeni, S. Bianchi, G. Vizsnyiczai, M. L. Bernardini, and R. Di Leonardo, Dynamic density shaping of photokinetic *E. coli*, *eLife* **7**, e36608 (2018).
- [97] P. G. de Gennes and J. Prost, *The Physics of Liquid Crystals* (Oxford University Press, New York, 1993).
- [98] M. M. Genkin, A. Sokolov, O. D. Lavrentovich, and I. S. Aranson, Topological Defects in a Living Nematic Ensnare Swimming Bacteria, *Phys. Rev. X* **7**, 011029 (2017).
- [99] A. Doostmohammadi, M. F. Adamer, S. P. Thampi, and J. M. Yeomans, Stabilization of active matter by flow-vortex lattices and defect ordering, *Nat. Commun.* **7**, 10557 (2016).
- [100] T. Ishikawa, N. Yoshida, H. Ueno, M. Wiedeman, Y. Imai, and T. Yamaguchi, Energy Transport in a Concentrated Suspension of Bacteria, *Phys. Rev. Lett.* **107**, 028102 (2011).
- [101] T. N. Shendruk, K. Thijssen, J. M. Yeomans, and A. Doostmohammadi, Twist-induced crossover from two-dimensional to three-dimensional turbulence in active nematics, *Phys. Rev. E* **98**, 010601 (2018).
- [102] J. Elgeti and G. Gompper, Emergence of metachronal waves in cilia arrays, *Proc. Natl. Acad. Sci. U.S.A.* **110**, 4470 (2013).
- [103] Y. Ding, J. C. Nawroth, M. J. McFall-Ngai, and E. Kanso, Mixing and transport by ciliary carpets: a numerical study, *J. Fluid Mech.* **743**, 124 (2014).
- [104] N. Uchida and R. Golestanian, Synchronization and collective dynamics in a carpet of microfluidic rotors, *Phys. Rev. Lett.* **104**, 178103 (2010).
- [105] N. Uchida and R. Golestanian, Synchronization in a carpet of hydrodynamically coupled rotors with random intrinsic frequency, *Europhys. Lett.* **89**, 50011 (2010).
- [106] N. Darnton, L. Turner, K. Breuer, and H. C. Berg, Moving fluid with bacterial carpets, *Biophys. J.* **86**, 1863 (2004).
- [107] M. J. Kim and K. S. Breuer, Microfluidic pump powered by self-organizing bacteria, *Small* **4**, 111 (2008).
- [108] Y.-T. Hsiao, J.-H. Wang, K.-T. Wu, J. Tsai, C.-H. Chang, and W.-Y. Woon, Collective flow dynamics across a bacterial carpet: Understanding the forces generated, *Appl. Phys. Lett.* **105**, 203702 (2014).
- [109] Y.-T. Hsiao, K.-T. Wu, N. Uchida, and W.-Y. Woon, Impurity-tuned non-equilibrium phase transition in a bacterial carpet, *Appl. Phys. Lett.* **108**, 183701 (2016).
- [110] H. C. F. Marcos, T. R. Powers, and R. Stocker, Bacterial rheotaxis, *Proc. Natl. Acad. Sci. U.S.A.* **109**, 4780 (2012).
- [111] R. A. Simha and S. Ramaswamy, Hydrodynamic Fluctuations and Instabilities in Ordered Suspensions of Self-Propelled Particles, *Phys. Rev. Lett.* **89**, 058101 (2002).
- [112] I. D. Vladescu, E. J. Marsden, J. Schwarz-Linek, V. A. Martinez, J. Arlt, A. N. Morozov, D. Marenduzzo, M. E. Cates, and W. C. K. Poon, Filling an Emulsion Drop with Motile Bacteria, *Phys. Rev. Lett.* **113**, 268101 (2014).
- [113] L. M. Janssen, A. Kaiser, and H. Löwen, Aging and rejuvenation of active matter under topological constraints, *Sci. Rep.* **7**, 5667 (2017).
- [114] P. Galajda, J. Keymer, P. Chaikin, and R. Austin, A wall of funnels concentrates swimming bacteria, *J. Bacteriol.* **189**, 8704 (2007).
- [115] M. B. Wan, C. J. Olson Reichhardt, Z. Nussinov, and C. Reichhardt, Rectification of Swimming Bacteria and Self-Driven Particle Systems by Arrays of Asymmetric Barriers, *Phys. Rev. Lett.* **101**, 018102 (2008).
- [116] N. Koumakis, A. Lepore, C. Maggi, and R. Di Leonardo, Targeted delivery of colloids by swimming bacteria, *Nat. Commun.* **4**, 2588 (2013).
- [117] J. Simmchen, J. Katuri, W. E. Uspal, M. N. Popescu, M. Tasinkevych, and S. Sánchez, Topographical pathways guide chemical microswimmers, *Nat. Commun.* **7**, 10598 (2016).
- [118] F. G. Woodhouse, A. Forrow, J. B. Fawcett, and J. Dunkel, Stochastic cycle selection in active flow networks, *Proc. Natl. Acad. Sci. U.S.A.* **113**, 8200 (2016).
- [119] L. Vidakovic, P. K. Singh, R. Hartmann, C. D. Nadell, and K. Drescher, Dynamic biofilm architecture confers individual and collective mechanisms of viral protection, *Nat. Rev. Microbiol.* **3**, 26 (2018).